

Flat surface state with octupole moment in an e_g orbital system on a simple cubic lattice

Katsunori Kubo

Advanced Science Research Center, Japan Atomic Energy Agency, Tokai, Ibaraki 319-1195, Japan
(Dated: August 23, 2024)

A tight-binding model for e_g orbitals on a simple cubic lattice with finite thickness is investigated. The hopping integrals for nearest-neighboring sites are considered. We examine the electronic band structures for systems with (001), (110), and (111) surfaces. Electronic states well localized around the surfaces are found for the (110) and (111) surfaces. In particular, the surface state is flat and extends in the entire Brillouin zone for the (111) surface, provided the bulk band projected onto the surface Brillouin zone is gapped. We also find that these surface states possess octupole moments in both the (110) and (111) surface cases.

I. INTRODUCTION

Topological semimetals are distinguished by the topological protection of band degeneracies, which can occur at discrete points, known as Dirac or Weyl points [1–4], or along continuous lines, referred to as topological nodal lines [5–7]. These materials have attracted considerable attention due to their unique and fascinating physical properties.

Achieving such topological features requires at least two electronic bands. In systems with two atomic sites per unit cell, such as honeycomb and diamond lattices, this condition is naturally met, leading to the presence of Dirac points [1, 2] and nodal lines [8], respectively. Another approach involves leveraging the spin degrees of freedom. For example, Rashba spin-orbit coupling [9] can lift the spin degeneracy of a band, except at specific \mathbf{k} points where time-reversal symmetry ensures degeneracy, resulting in Weyl points [10].

Another possibility is to use the orbital degrees of freedom. We examine the e_g orbitals of d electrons as a prototypical example of two-orbital systems. Indeed, Dirac points have been investigated in two-dimensional e_g orbital systems [11–14]. In particular, in our previous study [14], we found edge states in an e_g orbital model on a square lattice, similar to the single-orbital honeycomb lattice model [15]. The edge state in the e_g orbital model possesses an octupole moment.

Here, we extend the e_g orbital model to a three-dimensional system, specifically on a simple cubic lattice. We find topological nodal lines in this model. In the presence of such topological nodal lines, surface states are expected [5–7]. For example, in a single-orbital tight-binding model on a diamond lattice, a flat surface state appears on the (111) surface [16, 17]. In our model, we find flat surface states in the entire Brillouin zone for the (111) surface as long as the bulk band projected onto the surface Brillouin zone is gapped. This contrasts with the single-orbital model on a diamond lattice, where the flat surface state appears only in a part of the surface Brillouin zone. Additionally, the surface state in our model possesses an octupole moment.

II. MODEL

In this paper, we omit considerations of a magnetic field and magnetic ordering. Consequently, we can disregard the spin degrees of freedom and reduce our model to a spinless one. The Hamiltonian for a simple cubic lattice with nearest-neighbor hopping is given by

$$H = \sum_{\tau\tau'} c_{\mathbf{k}\tau}^\dagger \epsilon_{\tau\tau'}(\mathbf{k}) c_{\mathbf{k}\tau'}, \quad (1)$$

where $c_{\mathbf{k}\tau}$ is the annihilation operator for an electron with momentum \mathbf{k} and orbital τ . Here, $\tau = 1$ corresponds to the $x^2 - y^2$ orbital and $\tau = 2$ corresponds to the $3z^2 - r^2$ orbital. The matrix elements of the Hamiltonian are given by [18, 19]

$$\epsilon_{11}(\mathbf{k}) = \frac{1}{2}[3(dd\sigma) + (dd\delta)](c_x + c_y) + 2(dd\delta)c_z, \quad (2)$$

$$\epsilon_{22}(\mathbf{k}) = \frac{1}{2}[(dd\sigma) + 3(dd\delta)](c_x + c_y) + 2(dd\sigma)c_z, \quad (3)$$

$$\epsilon_{12}(\mathbf{k}) = \epsilon_{21}(\mathbf{k}) = -\frac{\sqrt{3}}{2}[(dd\sigma) - (dd\delta)](c_x - c_y), \quad (4)$$

where $c_\mu = \cos k_\mu a$ with $\mu = x, y, z$, and a is the lattice constant. $(dd\sigma)$ and $(dd\delta)$ represent the two-center integrals [20]. This model can be adapted to Γ_8 orbitals of f electrons by substituting $(dd\sigma)$ with $[3(ff\sigma) + 4(ff\pi)]/7$ and $(dd\delta)$ with $[(ff\pi) + 5(ff\delta) + 15(ff\phi)]/21$. Since the model is for two orbitals, the matrix $\epsilon(\mathbf{k})$ can be expressed using the Pauli matrices:

$$\begin{aligned} \epsilon(\mathbf{k}) &= \frac{1}{2}[\epsilon_{11}(\mathbf{k}) + \epsilon_{22}(\mathbf{k})]\sigma^0 \\ &\quad + \frac{1}{2}[\epsilon_{11}(\mathbf{k}) - \epsilon_{22}(\mathbf{k})]\sigma^z + \epsilon_{12}(\mathbf{k})\sigma^x \\ &= h_0(\mathbf{k})\sigma^0 + h_x(\mathbf{k})\sigma^x + h_z(\mathbf{k})\sigma^z, \end{aligned} \quad (5)$$

where σ^μ denotes the μ component of the Pauli matrix, and σ^0 is the identity matrix. The coefficients are given

by:

$$\begin{aligned} h_0(\mathbf{k}) &= [\epsilon_{11}(\mathbf{k}) + \epsilon_{22}(\mathbf{k})]/2 \\ &= [(dd\sigma) + (dd\delta)](c_x + c_y + c_z) \\ &= 2t_1(c_x + c_y + c_z), \end{aligned} \quad (6)$$

$$\begin{aligned} h_x(\mathbf{k}) &= \epsilon_{12}(\mathbf{k}) = \epsilon_{21}(\mathbf{k}) \\ &= -\frac{\sqrt{3}}{2}[(dd\sigma) - (dd\delta)](c_x - c_y) \\ &= -\sqrt{3}t_2(c_x - c_y), \end{aligned} \quad (7)$$

$$\begin{aligned} h_z(\mathbf{k}) &= [\epsilon_{11}(\mathbf{k}) - \epsilon_{22}(\mathbf{k})]/2 \\ &= \frac{1}{2}[(dd\sigma) - (dd\delta)](c_x + c_y - 2c_z) \\ &= t_2(c_x + c_y - 2c_z). \end{aligned} \quad (8)$$

We define the parameters:

$$t_1 = [(dd\sigma) + (dd\delta)]/2, \quad (9)$$

$$t_2 = [(dd\sigma) - (dd\delta)]/2, \quad (10)$$

and assume $t_1 \geq 0$ and $t_2 \geq 0$ without loss of generality. Thus, we parametrize them as

$$t_1 = t \cos \alpha, \quad (11)$$

$$t_2 = t \sin \alpha, \quad (12)$$

with $t > 0$ and $0 \leq \alpha \leq \pi/2$.

This model has been studied across various contexts with different values of α . For $\alpha = 0$ [$t_2 = 0$, $(dd\delta) = (dd\sigma)$, see Fig. 1(a)], the potential for anisotropic superconducting pairing arising from the orbital anisotropy of e_g orbitals has been explored [21]. Such anisotropic superconductivity has been investigated in the f -electron system $\text{PrT}_2\text{X}_{20}$ (where T is a transition metal and X is Zn or Al) [22–25]. For $\alpha = \pi/4$ [$t_1 = t_2$, $(dd\delta) = 0$], the model has been applied to perovskite manganites [26] and to the Γ_8 orbitals of f electrons, considering only ($ff\sigma$) [22–25, 27–34]. An effective Hamiltonian in the strong coupling limit is derived from this model, and frustration arising from the orbital anisotropy is discussed [35–39]. A similar frustrated model is known as the Kitaev model, which has been the subject of extensive study [40, 41]. In the two-dimensional version of the model for $\alpha = \pi/2$ [$t_1 = 0$, $(dd\delta) = -(dd\sigma)$, see Fig. 1(d)] near half filling, pocket Fermi surfaces appear around $(\pm\pi/2, \pm\pi/2)$. If a superconducting pair consists of electrons on the same Fermi pocket, the superconducting pair will possess a finite total momentum (π, π) , akin to the Fulde-Ferrell-Larkin-Ovchinnikov state [42, 43], even in the absence of a magnetic field, resembling the η -pairing state [44]. This possibility has been examined in Refs. [18, 19].

The energy dispersion of the model is given by

$$\begin{aligned} E(\mathbf{k}) &= h_0(\mathbf{k}) \pm \sqrt{h_x^2(\mathbf{k}) + h_z^2(\mathbf{k})} \\ &= h_0(\mathbf{k}) \pm h(\mathbf{k}). \end{aligned} \quad (13)$$

Note that hybridization between the $x^2 - y^2$ and $3z^2 - r^2$ orbitals is prohibited on the $k_x = k_y$ plane due to

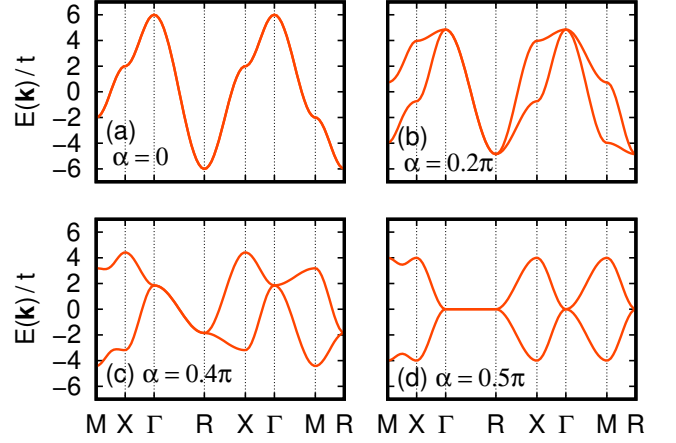


FIG. 1. Energy dispersion along symmetric directions for (a) $\alpha = 0$, (b) $\alpha = 0.2\pi$, (c) $\alpha = 0.4\pi$, and (d) $\alpha = 0.5\pi$. The high-symmetry points are $\Gamma = (0, 0, 0)$, $X = (\pi/a, 0, 0)$, $M = (\pi/a, \pi/a, 0)$, and $R = (\pi/a, \pi/a, \pi/a)$.

mirror symmetry [11, 12]. Additionally, these orbitals are degenerate along the $k_x = k_y = k_z$ line. Consequently, the two bands intersect along this and equivalent lines, $(k_x, k_y, k_z) \parallel (\pm 1, \pm 1, \pm 1)$. These lines are topological nodal lines.

In Fig. 1, we show the energy dispersion for some values of α . The two bands are degenerate along the nodal line (Γ – R line). The bandwidth W varies non-monotonically with α : $W = 12t$ at $\alpha = 0$ [Fig. 1(a)], $W = 6\sqrt{2}t$ at $\alpha = 0.25\pi$, $W = 4\sqrt{5}t$ at $\alpha = \tan^{-1} 2 = 0.3524\pi$, and $W = 8t$ at $\alpha = 0.5\pi$ [Fig. 1(d)].

We can define the winding number w of the normalized two-component vector field $\hat{\mathbf{h}}(\mathbf{k}) = \mathbf{h}(\mathbf{k})/h(\mathbf{k}) = [h_x(\mathbf{k}), h_z(\mathbf{k})]/h(\mathbf{k}) = [\hat{h}_x(\mathbf{k}), \hat{h}_z(\mathbf{k})]$ as follows,

$$w = \oint_C \frac{d\mathbf{k}}{2\pi} \cdot [\hat{h}_x(\mathbf{k})\nabla\hat{h}_z(\mathbf{k}) - \hat{h}_z(\mathbf{k})\nabla\hat{h}_x(\mathbf{k})], \quad (14)$$

where C is a closed loop. For a loop encircling the nodal line $(0, 0, 0) - (a_x\pi/a, a_y\pi/a, a_z\pi/a)$ with $a_x, a_y, a_z = \pm 1$, we obtain $w = -a_x a_y a_z$.

In a model with finite thickness, i.e., with two parallel surfaces, we define the momentum \mathbf{k}_{\parallel} parallel to the surfaces. When \mathbf{k}_{\parallel} is fixed at a certain value, the system can be regarded as a one-dimensional system along the direction perpendicular to the surfaces. We denote the lattice constant of this one-dimensional model as \tilde{a} . The momentum k_{\perp} of this one-dimensional system is defined in the limit of infinite thickness. The winding number $w(\mathbf{k}_{\parallel})$ for the one-dimensional system is then given by

$$w(\mathbf{k}_{\parallel}) = \int_0^{2\pi/\tilde{a}} \frac{dk_{\perp}}{2\pi} \left[\hat{h}_x(\mathbf{k}) \frac{\partial}{\partial k_{\perp}} \hat{h}_z(\mathbf{k}) - \hat{h}_z(\mathbf{k}) \frac{\partial}{\partial k_{\perp}} \hat{h}_x(\mathbf{k}) \right]. \quad (15)$$

The multipole operators at site $(i, \mathbf{r}_{\parallel})$ are defined as

$$\hat{\sigma}^{\mu}(i, \mathbf{r}_{\parallel}) = \sum_{\tau\tau'} c_{i\mathbf{r}_{\parallel}\tau}^{\dagger} \sigma_{\tau\tau'}^{\mu} c_{i\mathbf{r}_{\parallel}\tau'}, \quad (16)$$

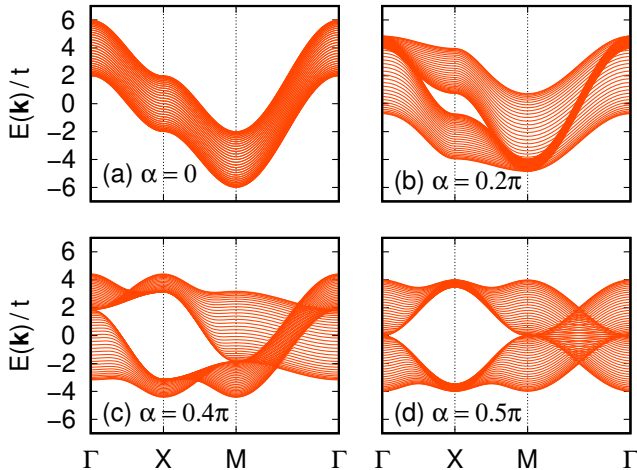


FIG. 2. Energy dispersion for a system with (001) surfaces along symmetric directions for (a) $\alpha = 0$, (b) $\alpha = 0.2\pi$, (c) $\alpha = 0.4\pi$, and (d) $\alpha = 0.5\pi$. The high-symmetry points are $\Gamma = (0, 0)$, $X = (\pi/a, 0)$, and $M = (\pi/a, \pi/a)$. The number of layers perpendicular to the surfaces is $L_z = 31$.

where \mathbf{r}_{\parallel} is the position vector parallel to the surfaces, i denotes the position perpendicular to the surfaces, $c_{i\mathbf{r}_{\parallel}\tau}$ is the annihilation operator of the electron at site $(i, \mathbf{r}_{\parallel})$ with orbital τ , and $\mu = 0, x, y, \text{ or } z$. The multipole operator at position i is given by

$$\begin{aligned} \hat{\sigma}^{\mu}(i) &= \sum_{\mathbf{r}_{\parallel}} \hat{\sigma}^{\mu}(i, \mathbf{r}_{\parallel}) \\ &= \sum_{\mathbf{k}_{\parallel}\tau\tau'} c_{i\mathbf{k}_{\parallel}\tau}^{\dagger} \sigma_{\tau\tau'}^{\mu} c_{i\mathbf{k}_{\parallel}\tau'} \\ &= \sum_{\mathbf{k}_{\parallel}} \hat{\sigma}^{\mu}(i, \mathbf{k}_{\parallel}), \end{aligned} \quad (17)$$

where $c_{i\mathbf{k}_{\parallel}\tau}$ is the Fourier transform of $c_{i\mathbf{r}_{\parallel}\tau}$ parallel to the surfaces. The zeroth component is the charge operator $\hat{Q}(i) = \hat{\sigma}^0(i)$, the z and x components are the quadrupole operators $\hat{O}_{20}(i) = \hat{\sigma}^z(i)$ and $\hat{O}_{22}(i) = \hat{\sigma}^x(i)$, respectively, and the y component is the octupole operator $\hat{T}_{xyz}(i) = \hat{\sigma}^y(i)$ [45, 46].

III. (001) SURFACE

For the (001) surface case, $\mathbf{k}_{\parallel} = (k_x, k_y)$ and $k_{\perp} = k_z$. The lattice constant in the direction perpendicular to the surfaces is $\tilde{a} = a$. We find $w(\mathbf{k}_{\parallel}) = 0$ in the entire surface Brillouin zone.

In Fig. 2, we show the energy dispersion for a lattice with a finite thickness of $\tilde{a}L_z$, where $L_z = 31$. As expected from $w(\mathbf{k}_{\parallel}) = 0$, we observe no surface states isolated from the bulk states.

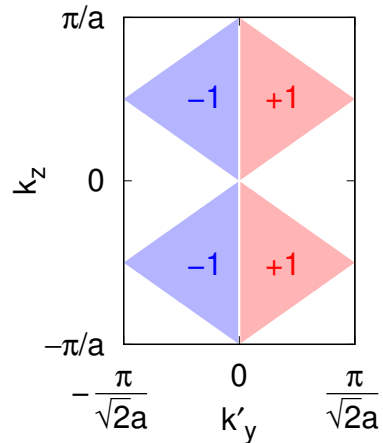


FIG. 3. Winding number $w(\mathbf{k}_{\parallel})$ in the first Brillouin zone for a system with (110) surfaces. The winding number $w(\mathbf{k}_{\parallel})$ is zero in the non-shaded areas.

IV. (110) SURFACE

For the (110) surface case, the lattice constant in the direction perpendicular to the surfaces is $\tilde{a} = a/\sqrt{2}$. We define $\mathbf{k}_{\parallel} = (k'_y, k_z)$ and $k_{\perp} = k'_x$, where k'_y is the momentum parallel to the surfaces and perpendicular to the z axis, and k'_x is the momentum perpendicular to the surfaces. The vector $\mathbf{h}(\mathbf{k})$ is expressed by using these momenta: $h_x(\mathbf{k}) = -2\sqrt{3}t_2 \sin(k'_x a/\sqrt{2}) \sin(k'_y a/\sqrt{2})$ and $h_z(\mathbf{k}) = 2t_2[\cos(k'_x a/\sqrt{2}) \cos(k'_y a/\sqrt{2}) - c_z]$.

In Fig. 3, we show the winding number $w(\mathbf{k}_{\parallel})$ in the surface Brillouin zone. In the region where $w(\mathbf{k}_{\parallel}) \neq 0$, we expect a surface state, provided that the bulk band projected onto the surface Brillouin zone is gapped.

In Fig. 4, we show the energy band for a lattice with a finite thickness $\tilde{a}L_{x'}$ with $L_{x'} = 31$. For $\alpha = 0$, all the bands are degenerate for $k'_y = \pi/\sqrt{2}a$. For $\alpha < \tan^{-1} 2 = 0.3524\pi$, the bulk band gap is closed in the region where $w(\mathbf{k}_{\parallel}) \neq 0$. For $\alpha > \tan^{-1} 2$, the bulk band gap opens except on the lines where $w(\mathbf{k}_{\parallel})$ changes. For $\alpha > \tan^{-1} 2$, we observe surface states isolated from the bulk band in parts of S - Γ and X - Y lines, as shown in Figs. 4(c) and 4(d). The appearance of the surface states is in accord with the $w(\mathbf{k}_{\parallel}) \neq 0$ region in Fig. 3.

For a fixed k_z , the model is reduced to a two-dimensional model with the difference in the energy levels of orbitals $\Delta = -4t_2c_z$ and an energy shift of $2t_1c_z$. Using the results of the two-dimensional model [14], we obtain the energy of the surface state: $E = -\Delta/\tan\alpha + 2t_1c_z = 6t_1c_z$. The energy dispersions of the surface state on the S - Γ and X - Y lines for $\alpha = 0.4\pi$ in Fig. 4(c) and for $\alpha = 0.5\pi$ in Fig. 4(d) are given by this equation.

From the results of the two-dimensional model, we also conclude that, at $(k'_y, k_z) = [\pi/(3\sqrt{2}a), \pi/(2a)]$, the surface state is completely localized on the first layer of the surface with a fully polarized octupole moment for

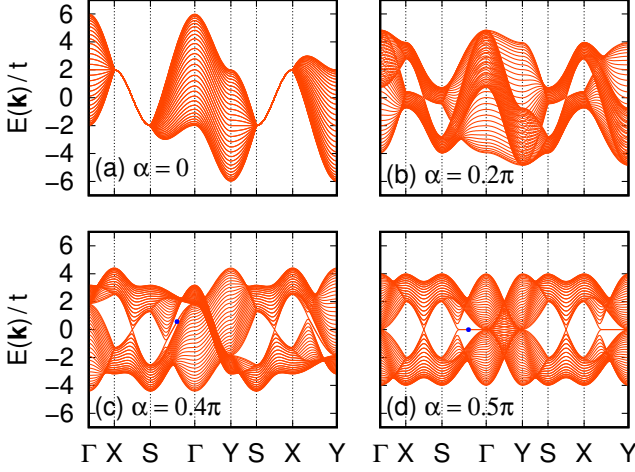


FIG. 4. Energy dispersion for a system with (110) surfaces along symmetric directions at (a) $\alpha = 0$, (b) $\alpha = 0.2\pi$, (c) $\alpha = 0.4\pi$, and (d) $\alpha = 0.5\pi$. The high-symmetry points are $\Gamma = (0, 0)$, $X = (\pi/\sqrt{2}a, 0)$, $Y = (0, \pi/a)$, and $S = (\pi/\sqrt{2}a, \pi/a)$. The number of layers perpendicular to the surfaces is $L_{x'} = 31$. The solid circles in (c) and (d) indicate the surface states in which the multipole density is evaluated in Figs. 5(a) and 5(b), respectively.

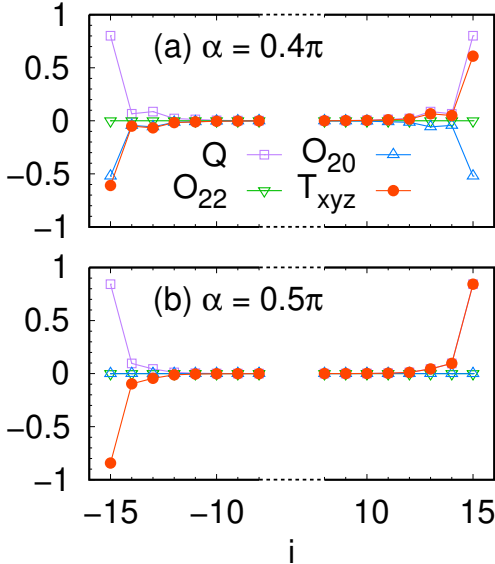


FIG. 5. Multipole density in the surface state for a lattice with (110) surfaces at $\mathbf{k}_{\parallel} = 0.4 \times S$ (a) for $\alpha = 0.4\pi$ [see Fig. 4(c)] and (b) for $\alpha = 0.5\pi$ [see Fig. 4(d)]. The number of layers perpendicular to the surfaces is $L_{x'} = 31$, and $S = (\pi/\sqrt{2}a, \pi/a)$.

$\alpha = 0.5\pi$. For other \mathbf{k}_{\parallel} and α , we need to evaluate the multipole density numerically.

We show the multipole density around the surfaces for $\alpha = 0.4\pi$ in Fig. 5(a) and for $\alpha = 0.5\pi$ in Fig. 5(b) at $\mathbf{k}_{\parallel} = 0.4 \times S$ with $S = (\pi/\sqrt{2}a, \pi/a)$. The surface

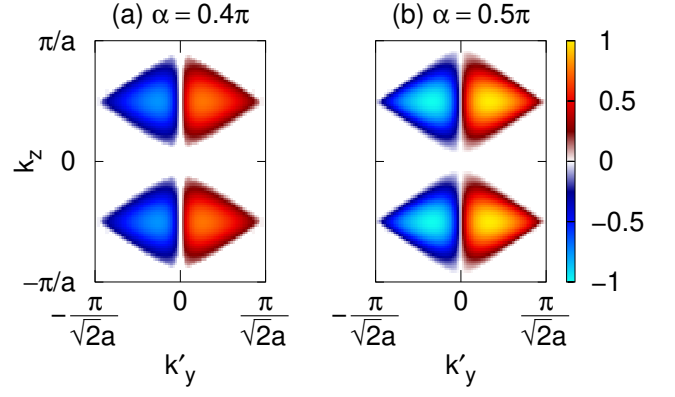


FIG. 6. Octupole density on the top layer $i = (L_{x'} - 1)/2$ of the (110) surface in the surface state (a) for $\alpha = 0.4\pi$ and (b) for $\alpha = 0.5\pi$. The number of layers perpendicular to the surfaces is $L_{x'} = 101$.

states are doubly degenerate, and we show the total multipole density of these two states. From the charge density $Q(i) = \langle \hat{Q}(i) \rangle$, where $\langle \dots \rangle$ denotes the sum of the expectation values in the two surface states, we recognize that these states are localized around the surfaces. $O_{22}(i) = \langle \hat{Q}_{22}(i) \rangle$ is always zero, and $O_{20}(i) = \langle \hat{Q}_{20}(i) \rangle$ is also zero for $\alpha = 0.5\pi$. The octupole moment $T_{xyz}(i) = \langle \hat{T}_{xyz}(i) \rangle$ is opposite between the surfaces.

In Fig. 6, we show the octupole density on the top layer $i = (L_{x'} - 1)/2$ in the surface state. As we noted, at $(k'_y, k_z) = [\pi/(3\sqrt{2}a), \pi/(2a)]$ (at the center of mass of the triangle) for $\alpha = 0.5\pi$, the octupole density reaches unity.

V. (111) SURFACE

For the (111) surface case, the lattice constant in the direction perpendicular to the surfaces is $\tilde{a} = a/\sqrt{3}$. We define $\mathbf{k}_{\parallel} = (k'_x, k'_y)$ and $k_{\perp} = k'_z$. The top layer of the (111) surface forms a triangular lattice. Here, k'_x is the momentum parallel to one of the edges of a triangle in the triangular lattice, k'_y is the momentum parallel to the surfaces and perpendicular to the k'_x axis, and k'_z is the momentum perpendicular to the surfaces. The vector $\mathbf{h}(\mathbf{k})$ is expressed using these momenta as follows: $h_x(\mathbf{k}) = 2\sqrt{3}t_2 \sin(k'_x a/\sqrt{2}) \sin(k'_y a/\sqrt{6} - k'_z a/\sqrt{3})$ and $h_z(\mathbf{k}) = 2t_2 [\cos(k'_x a/\sqrt{2}) \cos(k'_y a/\sqrt{6} - k'_z a/\sqrt{3}) - \cos(2k'_y a/\sqrt{6} + k'_z a/\sqrt{3})]$.

In Fig. 7, we show the winding number $w(\mathbf{k}_{\parallel})$ in the reciprocal space parallel to the surfaces. The winding number is nonzero except along the Γ - M $[(0, 0) - (0, \sqrt{2}\pi/\sqrt{3}a)]$ and equivalent lines. Thus, we expect a surface state at any \mathbf{k}_{\parallel} as long as the bulk band projected onto the surface Brillouin zone is gapped there.

In Fig. 8, we show the energy band for a lattice with a finite thickness $\tilde{a}L_{z'}$, with $L_{z'} = 31$. The size effect

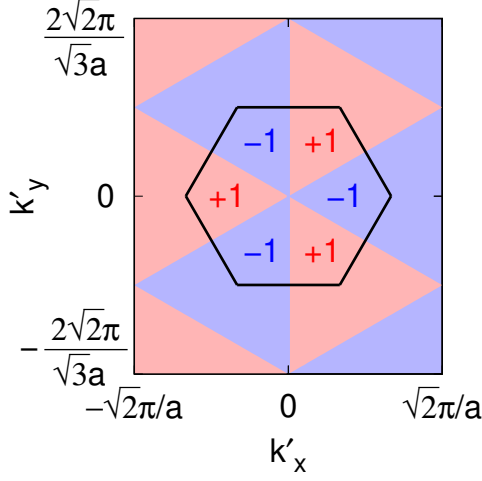


FIG. 7. Winding number $w(\mathbf{k}_{\parallel})$ for a system with (111) surfaces. The area enclosed by the solid line is the first Brillouin zone.

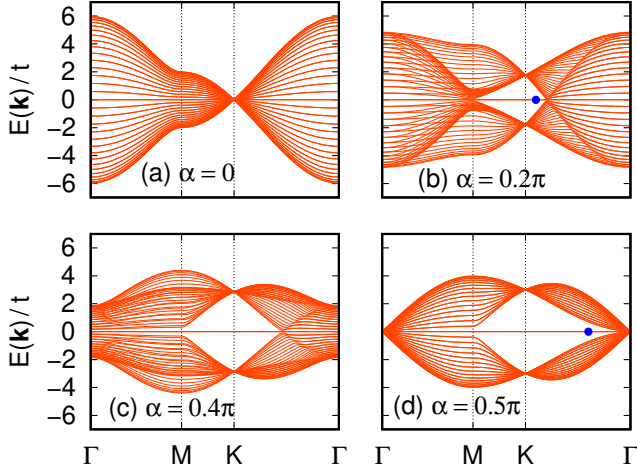


FIG. 8. Energy dispersion for a system with (111) surfaces along symmetric directions at (a) $\alpha = 0$, (b) $\alpha = 0.2\pi$, (c) $\alpha = 0.4\pi$, and (d) $\alpha = 0.5\pi$. The high-symmetry points are $\Gamma = (0, 0)$, $M = (0, \sqrt{2}\pi/\sqrt{3}a)$, and $K = (\sqrt{2}\pi/3a, \sqrt{2}\pi/\sqrt{3}a)$. The number of layers perpendicular to the surfaces is $L_{z'} = 31$. The solid circles in (b) and (d) indicate the surface states in which the multipole density is evaluated in Figs. 9(a) and 9(b), respectively.

is large around the M point for even numbers of $L_{z'}$; therefore, we have chosen $L_{z'} = 31$. We observe the flat surface state isolated from the bulk band when the bulk band gap opens. In particular, for $\alpha = 0.5\pi$, the flat surface state extends in the entire Brillouin zone except on the lines where $w(\mathbf{k}_{\parallel})$ changes.

We can show that the surface state is completely localized on the first layer of the surface with a fully polarized octupole moment at K point, irrespective of the value of α . At other \mathbf{k}_{\parallel} , we need to evaluate the multipole density numerically.

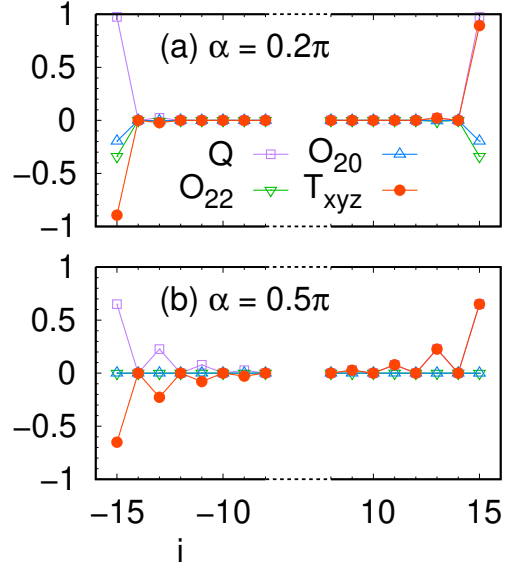


FIG. 9. Multipole density in the surface state for a system with (111) surfaces (a) for $\alpha = 0.2\pi$ at $\mathbf{k}_{\parallel} = 0.9 \times K$ [see Fig. 8(b)] and (b) for $\alpha = 0.5\pi$ at $\mathbf{k}_{\parallel} = 0.4 \times K$ [see Fig. 8(d)]. The number of layers perpendicular to the surfaces is $L_{z'} = 31$, and $K = (\sqrt{2}\pi/3a, \sqrt{2}\pi/\sqrt{3}a)$.

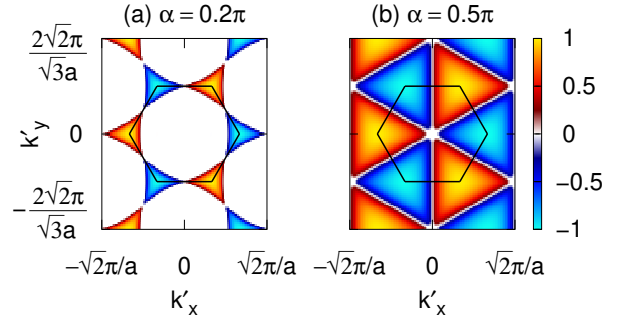


FIG. 10. Octupole density on the top layer $i = (L_{z'} - 1)/2$ of the (111) surface in the surface state (a) for $\alpha = 0.2\pi$ and (b) for $\alpha = 0.5\pi$. The number of layers perpendicular to the surfaces is $L_{z'} = 101$.

We show the multipole density around the surfaces for $\alpha = 0.2\pi$ in Fig. 9(a) and for $\alpha = 0.5\pi$ in Fig. 9(b). The surface states are doubly degenerate, and we show the total multipole density of these two states. From the charge density $Q(i)$, we recognize that these states are localized around the surfaces. $O_{20}(i)$ and $O_{22}(i)$ are zero for $\alpha = 0.5\pi$. The octupole moment $T_{xyz}(i)$ is opposite between the surfaces.

In Fig. 10, we show the octupole density on the top layer $i = (L_{z'} - 1)/2$ in the surface state. The octupole moment reaches unity at K point, irrespective of the value of α .

VI. SUMMARY AND DISCUSSION

We have investigated the surface states of an e_g orbital model on a simple cubic lattice. We find surface states with octupole moments on the (110) and (111) surfaces.

Concerning octupole moments, ordering of them has been observed in f -electron materials, such as NpO_2 [28, 30, 31, 47–51] and $\text{Ce}_x\text{La}_{1-x}\text{B}_6$ [52–57]. In e_g orbital systems of d electrons, the possibility of octupole ordering in the bulk perovskite manganites has been theoretically explored [45, 58–60]. However, a theory that incorporates fluctuations beyond the mean-field approximation concluded that such ordering is improbable [39, 46, 61]. The present paper uncovers the potential for octupole moments to emerge on the surfaces of e_g orbital systems.

Another characteristic of the surface state is the region in which it appears. The flat surface state appears on the

(111) surface across all surface momenta, provided the bulk band gap is open. This contrasts with the surface state of the single-orbital model on a diamond lattice with nearest-neighbor hopping, where the surface state emerges only in specific regions of the surface Brillouin zone [16].

As a candidate material, BaFeO_3 is promising [62]. This material crystallizes in the perovskite structure, with the Fe^{4+} ion possessing a $3d^4$ electron configuration. The ground state is ferromagnetic. Assuming the spins are fully polarized, the present spinless model can be applied to the half-filled e_g orbitals, while the wholly filled t_{2g} orbitals can be ignored.

ACKNOWLEDGMENTS

This work was supported by JSPS KAKENHI Grant No. JP23K03330.

-
- [1] P. R. Wallace, The Band Theory of Graphite, *Phys. Rev.* **71**, 622 (1947).
- [2] K. S. Novoselov, A. K. Geim, S. V. Morozov, D. Jiang, M. I. Katsnelson, I. V. Grigorieva, S. V. Dubonos, and A. A. Firsov, Two-dimensional gas of massless Dirac fermions in graphene, *Nature* **438**, 197 (2005).
- [3] S. Murakami, Phase transition between the quantum spin Hall and insulator phases in 3D: Emergence of a topological gapless phase, *New J. Phys.* **9**, 356 (2007).
- [4] X. Wan, A. M. Turner, A. Vishwanath, and S. Y. Savrasov, Topological semimetal and Fermi-arc surface states in the electronic structure of pyrochlore iridates, *Phys. Rev. B* **83**, 205101 (2011).
- [5] T. T. Heikkilä and G. E. Volovik, Dimensional crossover in topological matter: Evolution of the multiple Dirac point in the layered system to the flat band on the surface, *JETP Lett.* **93**, 59 (2011).
- [6] A. A. Burkov, M. D. Hook, and L. Balents, Topological nodal semimetals, *Phys. Rev. B* **84**, 235126 (2011).
- [7] H. Weng, Y. Liang, Q. Xu, R. Yu, Z. Fang, X. Dai, and Y. Kawazoe, Topological node-line semimetal in three-dimensional graphene networks, *Phys. Rev. B* **92**, 045108 (2015).
- [8] D. J. Chadi and M. L. Cohen, Tight-binding calculations of the valence bands of diamond and zincblende crystals, *Phys. Status Solidi B* **68**, 405 (1975).
- [9] Y. A. Bychkov and E. I. Rashba, Properties of a 2D electron gas with lifted spectral degeneracy, *JETP Lett.* **39**, 78 (1984).
- [10] K. Kubo, Weyl Semimetallic State in the Rashba–Hubbard Model, *J. Phys. Soc. Jpn.* **93**, 024708 (2024).
- [11] C. B. Bishop, G. Liu, E. Dagotto, and A. Moreo, On-site attractive multiorbital Hamiltonian for d -wave superconductors, *Phys. Rev. B* **93**, 224519 (2016).
- [12] M. Horio, C. E. Matt, K. Kramer, D. Sutter, A. M. Cook, Y. Sassa, K. Hauser, M. Månsson, N. C. Plumb, M. Shi, O. J. Lipscombe, S. M. Hayden, T. Neupert, and J. Chang, Two-dimensional type-II Dirac fermions in layered oxides, *Nat. Commun.* **9**, 3252 (2018).
- [13] L. L. Tao and E. Y. Tsymlal, Two-dimensional type-II Dirac fermions in a $\text{LaAlO}_3/\text{LaNiO}_3/\text{LaAlO}_3$ quantum well, *Phys. Rev. B* **98**, 121102(R) (2018).
- [14] K. Kubo, Octupolar edge state in an e_g orbital system on a square lattice, *Phys. Rev. B* **110**, 075110 (2024).
- [15] M. Fujita, K. Wakabayashi, K. Nakada, and K. Kusakabe, Peculiar Localized State at Zigzag Graphite Edge, *J. Phys. Soc. Jpn.* **65**, 1920 (1996).
- [16] Y. Takagi and S. Okada, Topologically induced surface electron state on Si(111) surfaces, *Surf. Sci.* **602**, 2876 (2008).
- [17] R. Takahashi and S. Murakami, Completely flat bands and fully localized states on surfaces of anisotropic diamond-lattice models, *Phys. Rev. B* **88**, 235303 (2013).
- [18] K. Kubo, Fulde–Ferrell–Larkin–Ovchinnikov State in the Absence of a Magnetic Field, *J. Phys. Soc. Jpn.* **77**, 043702 (2008).
- [19] K. Kubo, Superconductivity in e_g orbital systems with multi-Fermi-surface, *J. Optoelectron. Adv. Mater.* **10**, 1683 (2008).
- [20] J. C. Slater and G. F. Koster, Simplified LCAO Method for the Periodic Potential Problem, *Phys. Rev.* **94**, 1498 (1954).
- [21] K. Kubo, Pairing symmetry in a two-orbital Hubbard model on a square lattice, *Phys. Rev. B* **75**, 224509 (2007).
- [22] K. Kubo, Anisotropic Superconductivity Emerging from the Orbital Degrees of Freedom in a Γ_3 Non-Kramers Doublet System, *J. Phys. Soc. Jpn.* **87**, 073701 (2018).
- [23] K. Kubo, Superconductivity in a multiorbital model for the Γ_3 crystalline electric field state, *AIP Adv.* **8**, 101313 (2018).
- [24] K. Kubo, Nematic and time-reversal breaking superconductivities coexisting with quadrupole order in a Γ_3 system, *Phys. Rev. B* **101**, 064512 (2020).
- [25] K. Kubo, Coexistence of Superconductivity

- ity with Quadrupole Order in a Γ_3 System, JPS Conf. Proc. **30**, 011041 (2020).
- [26] P. W. Anderson, New Approach to the Theory of Superexchange Interactions, Phys. Rev. **115**, 2 (1959).
- [27] T. Hotta and K. Ueda, Construction of a microscopic model for f -electron systems on the basis of a j - j coupling scheme, Phys. Rev. B **67**, 104518 (2003).
- [28] K. Kubo and T. Hotta, Multipole ordering in f -electron systems on the basis of a j - j coupling scheme, Phys. Rev. B **72**, 144401 (2005).
- [29] K. Kubo and T. Hotta, Orbital-Controlled Superconductivity in f -Electron Systems, J. Phys. Soc. Jpn. **75**, 083702 (2006).
- [30] K. Kubo and T. Hotta, Multipole ordering in f -electron systems, Physica B **378–380**, 1081 (2006).
- [31] K. Kubo and T. Hotta, Multipole Ordering and Fluctuations in f -Electron Systems, J. Phys. Soc. Jpn. **75 Suppl.**, 232 (2006).
- [32] K. Kubo and T. Hotta, Superconductivity in f -electron systems controlled by crystalline electric fields, J. Magn. Magn. Mater. **310**, 572 (2007).
- [33] K. Kubo and T. Hotta, Influence of lattice structure on multipole interactions in Γ_3 non-Kramers doublet systems, Phys. Rev. B **95**, 054425 (2017).
- [34] K. Kubo and T. Hotta, Multipole interactions of Γ_3 non-Kramers doublet systems on cubic lattices, J. Phys.: Conf. Ser. **969**, 012096 (2018).
- [35] S. Ishihara, J. Inoue, and S. Maekawa, Electronic structure and effective Hamiltonian in perovskite Mn oxides, Physica C **263**, 130 (1996).
- [36] S. Ishihara, J. Inoue, and S. Maekawa, Effective Hamiltonian in manganites: Study of the orbital and spin structures, Phys. Rev. B **55**, 8280 (1997).
- [37] J. van den Brink, P. Horsch, F. Mack, and A. M. Oleś, Orbital dynamics in ferromagnetic transition-metal oxides, Phys. Rev. B **59**, 6795 (1999).
- [38] K. Kubo, Quantum Fluctuation Induced Order in an Anisotropic Pseudospin Model, J. Phys. Soc. Jpn. **71**, 1308 (2002).
- [39] K. Kubo and D. S. Hirashima, Orbital orderings and excitations in ferromagnetic metallic manganites, J. Phys. Chem. Solids **63**, 1571 (2002).
- [40] A. Kitaev, Anyons in an exactly solved model and beyond, Ann. Phys. (N.Y.) **321**, 2 (2006).
- [41] G. Jackeli and G. Khaliullin, Mott Insulators in the Strong Spin-Orbit Coupling Limit: From Heisenberg to a Quantum Compass and Kitaev Models, Phys. Rev. Lett. **102**, 017205 (2009).
- [42] P. Fulde and R. A. Ferrell, Superconductivity in a Strong Spin-Exchange Field, Phys. Rev. **135**, A550 (1964).
- [43] A. I. Larkin and Y. N. Ovchinnikov, Inhomogeneous state of superconductors, Sov. Phys. JETP **20**, 762 (1965).
- [44] C. N. Yang, η pairing and off-diagonal long-range order in a Hubbard model, Phys. Rev. Lett. **63**, 2144 (1989).
- [45] A. Takahashi and H. Shiba, Possible Orbital Orderings in a Model of Metallic Double-Exchange Ferromagnets, J. Phys. Soc. Jpn. **69**, 3328 (2000).
- [46] K. Kubo and D. S. Hirashima, Orbital Orderings in Ferromagnetic Metallic Manganites, J. Phys. Soc. Jpn. **71**, 183 (2002).
- [47] J. A. Paixão, C. Detlefs, M. J. Longfield, R. Caciuffo, P. Santini, N. Bernhoeft, J. Rebizant, and G. H. Lander, Triple- q Octupolar Ordering in NpO_2 , Phys. Rev. Lett. **89**, 187202 (2002).
- [48] R. Caciuffo, J. A. Paixão, C. Detlefs, M. J. Longfield, P. Santini, N. Bernhoeft, J. Rebizant, and G. H. Lander, Multipolar ordering in NpO_2 below 25 K, J. Phys.: Condens. Matter **15**, S2287 (2003).
- [49] Y. Tokunaga, Y. Homma, S. Kambe, D. Aoki, H. Sakai, E. Yamamoto, A. Nakamura, Y. Shiokawa, R. E. Walstedt, and H. Yasuoka, NMR Evidence for Triple- q Multipole Structure in NpO_2 , Phys. Rev. Lett. **94**, 137209 (2005).
- [50] K. Kubo and T. Hotta, Microscopic theory of multipole ordering in NpO_2 , Phys. Rev. B **71**, 140404(R) (2005).
- [51] K. Kubo and T. Hotta, Analysis of f - p model for octupole ordering in NpO_2 , Phys. Rev. B **72**, 132411 (2005).
- [52] K. Kubo and Y. Kuramoto, Lattice Distortion and Octupole Ordering Model in $\text{Ce}_x\text{La}_{1-x}\text{B}_6$, J. Phys. Soc. Jpn. **72**, 1859 (2003).
- [53] K. Kubo and Y. Kuramoto, Octupole Ordering Model for the Phase IV of $\text{Ce}_x\text{La}_{1-x}\text{B}_6$, J. Phys. Soc. Jpn. **73**, 216 (2004).
- [54] T. Morie, T. Sakakibara, T. Tayama, and S. Kunii, Low-Temperature Magnetization Study on the Phase IV Ordering in $\text{Ce}_x\text{La}_{1-x}\text{B}_6$ under [111] Uniaxial Pressures, J. Phys. Soc. Jpn. **73**, 2381 (2004).
- [55] D. Mannix, Y. Tanaka, D. Carbone, N. Bernhoeft, and S. Kunii, Order Parameter Segregation in $\text{Ce}_{0.7}\text{La}_{0.3}\text{B}_6$: $4f$ Octopole and $5d$ Dipole Magnetic Order, Phys. Rev. Lett. **95**, 117206 (2005).
- [56] H. Kusunose and Y. Kuramoto, Evidence for Octupole Order in $\text{Ce}_{0.7}\text{La}_{0.3}\text{B}_6$ from Resonant X-ray Scattering, J. Phys. Soc. Jpn. **74**, 3139 (2005).
- [57] K. Kuwahara, K. Iwasa, M. Kohgi, N. Aso, M. Sera, and F. Iga, Detection of Neutron Scattering from Phase IV of $\text{Ce}_{0.7}\text{La}_{0.3}\text{B}_6$: A Confirmation of the Octupole Order, J. Phys. Soc. Jpn. **76**, 093702 (2007).
- [58] R. Maezono and N. Nagaosa, Complex orbital state in manganites, Phys. Rev. B **62**, 11576 (2000).
- [59] J. van den Brink and D. Khomskii, Orbital ordering of complex orbitals in doped Mott insulators, Phys. Rev. B **63**, 140416(R) (2001).
- [60] D. I. Khomskii, ORBITAL EFFECTS IN MANGANITES, Int. J. Mod. Phys. B **15**, 2665 (2001).
- [61] K. Kubo and D. S. Hirashima, Correlation Effect on Orbital Orderings in Ferromagnetic Metallic Manganites, J. Phys. Soc. Jpn. **71 Suppl.**, 151 (2002).
- [62] N. Hayashi, T. Yamamoto, H. Kageyama, M. Nishi, Y. Watanabe, T. Kawakami, Y. Matsushita, A. Fujimori, and M. Takano, BaFeO_3 : A Ferromagnetic Iron Oxide, Angew. Chem., Int. Ed. **50**, 12547 (2011).